

High Power 1300 nm Fabry-Perot and DFB Ridge Waveguide Lasers

D. Garbuzov^{a1}, M. Maiorov^a, R. Menna^a, A. Komissarov^a, V. Khalfin^b,
I. Kudryashov^a, A. Lunev^a, L. DiMarco^b, J. Connolly^a.

Princeton Lightwave Inc., 2601 U.S. Route 130 S, Cranbury, NJ 08512, USA

*Princeton Lightwave, Inc. contractors from Sarnoff Corporation, Princeton, NJ.

ABSTRACT

In this paper we summarize the results [1] on the development of high power 1300 nm ridge waveguide Fabry-Perot and distributed-feedback (DFB) lasers.

Improved performance of MOCVD grown InGaAsP/InP laser structures and optimization of the ridge waveguide design allowed us to achieve more than 800 mW output power from 1300 nm single mode Fabry-Perot lasers. Despite the fact that the beam aspect ratio for ridge lasers ($30^\circ \times 12^\circ$) is higher than that for buried devices, our modeling and experiments demonstrated that the fiber coupling efficiency of about 75-80% could be routinely achieved using a lensed fiber or a simple lens pair. Fiber power of higher than 600 mW was displayed.

Utilizing similar epitaxial structures and device geometry, the 1300 nm DFB lasers with output power of 500 mW have been fabricated. Analysis of the laser spectral characteristics shows that the high power DFB lasers can be separated into several groups. The single frequency spectral behavior was exhibited by about 20 % of all studied DFB lasers. For these lasers, side-mode suppression increases from 45 dB at low current up to 60 dB at maximum current. About 30 % of DFB lasers, at all driving currents, demonstrate multi-frequency spectra consisting of 4-8 longitudinal modes with mode spacing larger than that for Fabry-Perot lasers of the same cavity length. Both single frequency and multi frequency DFB lasers exhibit weak wavelength-temperature dependence and very low relative intensity noise (RIN) values.

Fabry-Perot and both types of DFB lasers can be used as pump sources for Raman amplifiers operating in the 1300 nm wavelength range where the use of EDFA is not feasible. In addition, the single-mode 1300 nm DFB lasers operating in the 500 mW power range are very attractive for new generation of the cable television transmission and local communication systems.

Keywords: ridge-waveguide 1310 nm high-power diode laser, distributed feedback laser, relative intensity noise.

1. INTRODUCTION

High power, narrow linewidth, and low noise single-mode InP-based diode lasers operating in the 1300 nm wavelength range have important applications in cable television transmission systems, local communication systems, and interferometric sensors. The previously reported maximum power for 1300 nm InGaAsP/InP DFB lasers is 315 mW CW [2]. This power level, when compared with recently reported power levels of 1 W for 14xx nm InGaAsP/InP single-mode pump lasers [3] and 440 mW for 1550 nm DFB lasers [4], indicates that significant improvements in performance of Fabry-Perot and DFB emitters operating at 13xx nm may also be realized.

Ridge waveguide (RWG) and buried heterostructure (BH) are the two main laser configurations used for fabrication of commercial single mode diode lasers. RWG design dominates for lasers emitting in 0.8-0.98 μm wavelength range, since for AlGaAs/InGaAs – based systems, employed for this wavelength range, the regrowth process is complicated [5]. In contrast, the 1.3-1.55 μm lasers employed for telecommunication applications were until recently mainly of the BH design [6-8]. One of the main reasons for this design preference is the fact that BH lasers have a significantly lower beam aspect ratio compared to RWG devices, which makes them more suitable for cheap systems employing butt coupling.

¹ phone (609) 925-8103; Fax (609)409-7022; <http://www.princetonlightwave.com>, e-mail: dgarbuzov@princetonlightwave.com

This bias to buried heterostructure structures had recently abated when Al-containing AlInAs / InGaAsP 1.3-1.55 μm emitters emerged in the telecom arena [9].

Recently, an advanced ridge-waveguide design, allowing for record output powers from single mode Fabry-Perot and DFB lasers [1, 3, 4], has been demonstrated. The choice of the RWG design for high-power operation is determined by such advances as:

1. Single step wafer growth process.
2. Controllable lateral index step providing single mode operation for devices with wide active region.
3. Higher reliability of lasers without current blocking layers.

One more advantage of the RWG device design is the absence of a blocking layer capacitance providing potential for ultra high-speed operation of such lasers [10].

The high aspect ratio was considered the main disadvantage of RWG design since cheap butt coupling schemes become impossible. This disadvantage, however, is crucial only for low cost, low power butt-coupled laser systems. For more expensive high-power devices, a high aspect ratio can be easily overcome by using a simple lens pair or lensed fiber, resulting in routinely obtained 70-80% coupling efficiency [1, 3, 4].

In this paper, we present single-spatial-mode 800 mW output power Fabry-Perot and 500 mW output power DFB lasers emitting in 1300 nm range. The overall performance of these lasers is comparable to that of the latest generation of high-power 14xx nm pump lasers and 1550 nm DFB lasers [3, 4].

2. LASER STRUCTURE, DEVICE FABRICATION, AND TEST TECHNIQUES

The laser structures for Fabry-Perot devices are grown by low-pressure metal organic chemical vapour deposition (LP-MOCVD) on n -InP substrates and contain a strained InGaAsP quantum well (QW) active region. Lateral mode confinement is provided by a dual-channel ridge waveguide structure prepared by conventional photolithography in conjunction with chemical etching. Single-mode operation for lasers with a ridge width from 3 to 5 μm is maintained by accurate control of the channel etch depth with the use of a grown-in etch-stop layer in the laser structure

For DFB lasers, the multiple quantum well (MQW) structures were grown in two growth steps. First, a base structure, which includes the MQW active region and stops after the InGaAsP grating layer was grown using conventional growth techniques. The strained MQW region was optimised to obtain a high slope efficiency for long cavity devices. First-order Bragg gratings were fabricated on the grating layer using holographic photolithography followed by reactive ion etching (RIE). After defining the grating in the epitaxial structure, the wafer had been placed back in the MOCVD system where the laser structure was completed by growing the p -InP cladding and p -InGaAs contact layers. The grating position and its corresponding tooth height were designed to provide product $\kappa L \approx 1$, where κ is the grating coupling coefficient and L is the cavity length.

In this work, we investigated Fabry-Perot and DFB lasers with cavity lengths of 2 and 3 mm. The front and rear facets of the devices were coated with low- and high-reflective coatings, respectively. The lasers were mounted p-side down

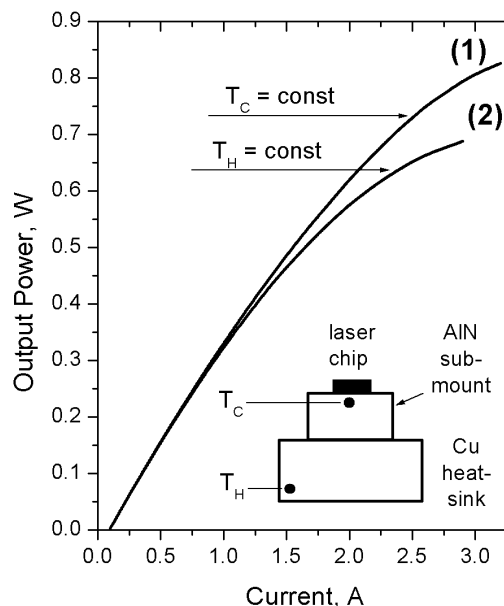


Fig.1. P-I characteristics of Fabry-Perot laser with cavity length of 3 mm measured at (1) stabilized temperature under the device active region, and (2) stabilized temperature of the water-cooled copper heatsink. Positions of temperature stabilization points are shown on the inset.

either in one step directly on standard copper C-blocks ($3.6 \times 6 \times 7$ mm) using In solder, or in two steps: first onto AlN or TcBN submounts using Au-Sn alloy solder, and then onto the C-blocks. C-blocks were bolted to copper heatsinks with thermal stabilization provided by either liquid coolant or high-performance thermo-electric cooler.

During our power-current (P-I) measurements with coolant-cooled heatsink, several small size thermocouples were used to map the temperature distribution across the top surface of the C-block. The temperature measurements demonstrated that C-block temperature increases considerably with increased driving current [1, 3]. The temperature distribution on the C-block surface weakly depends on the thermocouple position in the direction parallel to the laser axis, while in the perpendicular direction this dependence is much more pronounced. Using the approach presented in our previous paper [3], we estimated that the difference between thermal sensor reading and heatsink temperature directly under the RWG region of the device at 3 A driving current is about 15 °C. In order to improve temperature control, we placed an additional miniature thermocouple under the laser active region. The 125 μm diameter thermocouple was positioned in a micro ($d = 200 \mu\text{m}$) hole drilled in 0.9 mm thick AlN submount as shown in the inset of Fig. 1. Power-current (P-I) characteristics of the devices were measured under two conditions: (i) at constant temperature of the coolant flow, thus stabilizing the temperature (T_H) of the copper heatsink, and (ii) at the condition providing the constant value of temperature T_C measured under the laser. In the second case, a thermocouple mounted into AlN submount was inserted into the TEC feedback loop, thus providing stabilization of T_C .

3. MEASUREMENT RESULTS

Fig. 1 displays the P-I characteristics for one of the 1310 nm Fabry-Perot lasers with 3 mm cavity length. Curve (1) was measured with the TEC that supports the constant reading for thermocouple inserted in the AlN submount. Near-threshold efficiency of 380 mW/A and a maximum output power of 825 mW has been obtained at $T_C = 18^\circ\text{C}$. Under conditions of constant heatsink temperature (curve (2)), the thermal rollover of P-I curve was more pronounced and the power was 10-15% less in a 3 A current range.

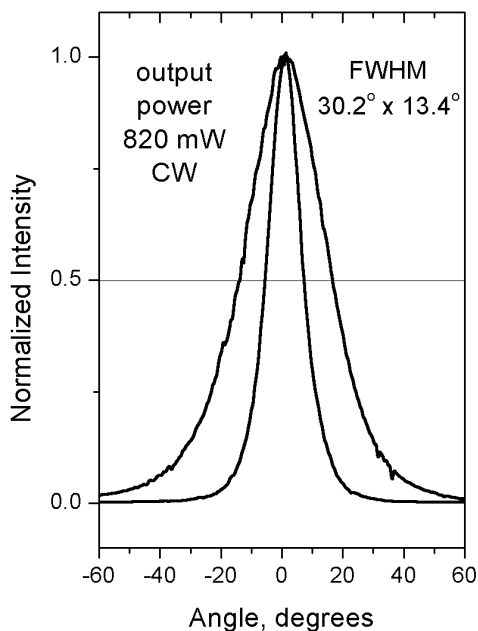


Fig.2. Slow and fast axis far-field patterns for Fabry-Perot lasers measured at output power of 820 mW

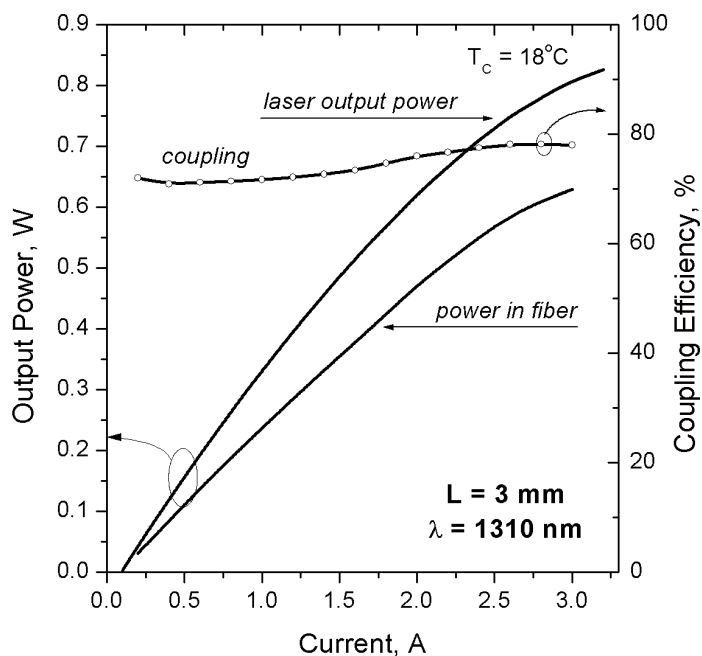


Fig.3. Ex-facet power, power in fiber, and coupling coefficient vs. current for $\lambda = 1310$ nm Fabry-Perot laser. The device was In-mounted p-side down onto copper C-block.

The far-field intensity distributions for the 1310 nm RWG Fabry-Perot laser operating at 820 mW is shown in Fig. 2. The full widths at half maximum (FWHM) of 13° (lateral) and 30° (perpendicular) are typical for high-power operation of the RWG emitters. The modest increase of the lateral far field FWHM from 11° to 13° with power increase from 200 to 800 mW was observed for most of the lasers tested. Overheating of the active region and temperature induced lateral refractive index gradients are the most likely causes for the observed lateral far field FWHM increase.

As the current increases from the threshold to 2 A, the laser spectrum shifts to longer wavelengths by 12-14 nm and broadens from 1-2 nm to 10-12 nm. Since spectrum stabilization is needed for Raman amplifier pump systems, fiber Bragg grating technique should be used to lock spectral distribution of Fabry-Perot lasers.

A simple aspherical lens pair (GelTech) has been used for radiation coupling into SMF-28 fiber with anti-reflective coatings on both fiber facets. Aperture of this lens pair reduces our coupling efficiency by about $\sim 6\%$. Despite this limitation, 78% coupling efficiency has been achieved for 1300 nm Fabry-Perot RWG emitters. Fig. 3 shows a modest increase in fiber coupling efficiency with increasing driving current due to the improvement of the aspect ratio for the output beam. The maximum optical power in fiber was 620 mW when the laser was operated under constant T_C conditions (Fig.3). To the best of our knowledge, 800 mW ex-facet and 620 mW ex-fiber powers are the highest levels reported for narrow-stripe lasers operating in the 1300 nm wavelength range.

4. DISTRIBUTED FEEDBACK LASERS

As well as in the case of the high power 14xx- 15xx nm Fabry-Perot and DFB lasers [3, 4], the structures similar to those designed for high power 1300 nm Fabry-Perot emitters, were used for fabricating DFB lasers operating in the same wavelength range [1]. The grating periods were selected to provide 1310 nm DFB operation.

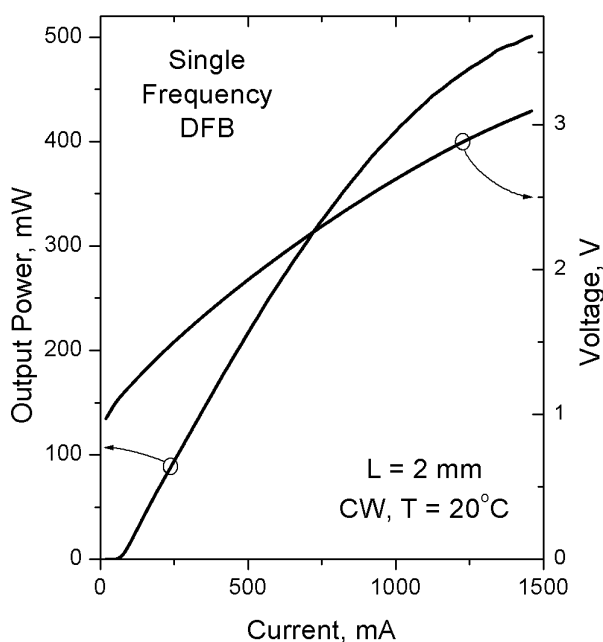


Fig.4. P-I-V characteristics of single frequency (group A) DFB laser with cavity length of 2 mm. The measurements were performed with heatsink temperature stabilization ($T_H = \text{const}$).

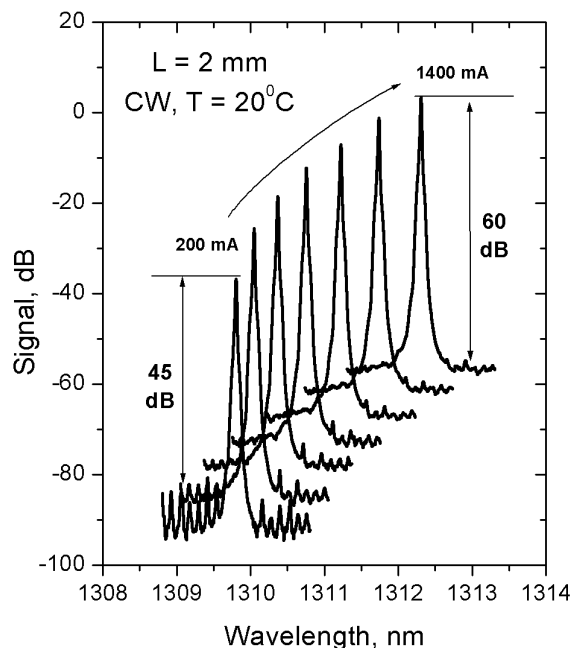


Fig.5. Spectral behaviour of single-frequency (group A) DFB laser with cavity length of 2mm. Side mode suppression ratio increases from 45 dB at 200 mA to more than 60 dB at 1400 mA drive current.

Analysis of P-I characteristics and spectra of the DFB lasers shows that the DFB devices can be separated into three distinct operating groups, which we will call A, B, and C. The ratio of the numbers of DFB devices in the groups A, B, and C approximately equals 2:3:5.

The feature of P-I characteristic of group "C" DFB lasers is the kinks that are associated with changes in the character of their spectra with current variation. DFB lasers from groups A and B display smooth P-I characteristics (Fig. 4, 6), but they have essentially different spectral distribution (Fig. 5, 7). Group A devices operate in single frequency (SF) mode with a side mode suppression ratio (SMSR) better than 60 dB, up to maximum output power, which is about 500 mW for the very best devices (Fig. 4, 5). More typical maximum power levels for 1310 nm SF DFBs are in the 440-480 mW range.

Figures 6 and 7 show P-I-V characteristics and spectra of multi-frequency (MF) DFB lasers (group B). The mode spacing for MF DFB lasers is about 1.5-3 Å, or about two-three times larger than mode spacing observed in conventional FP lasers of the same cavity length. The number of modes observed within a 60 dB intensity range increases from 3-5, near threshold, to 6-10 at maximum power levels. Current-induced wavelength shifts for SF and MF DFB lasers are shown in Fig. 8. The rate of spectrum shift with current for both types of 3 mm DFB lasers is about 0.012 Å/mA, which is 5-6 times less than that for similar FP lasers. Temperature measurements clearly demonstrate spectrum stabilization for both types of DFB lasers. SF mode operation was observed up to 75°C with 50% output power reduction at 60°C for 1 A driving current.

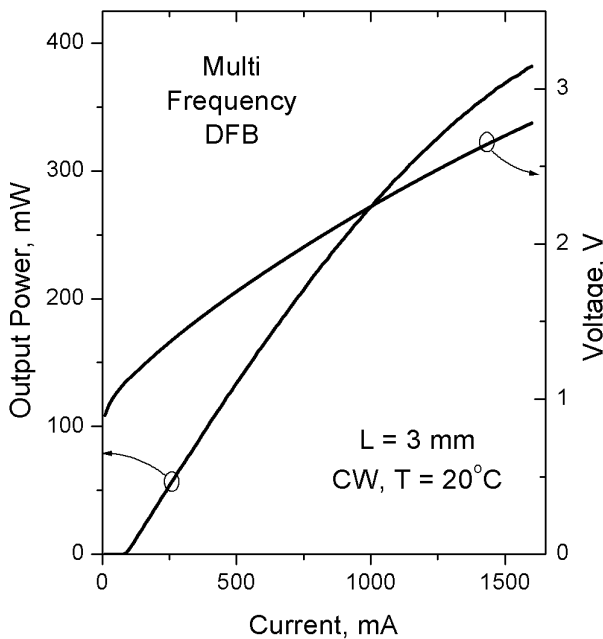


Fig.6. P-I and I-V characteristics of multi-frequency (group B) DFB laser with cavity length of 3 mm. The measurements were performed with heatsink temperature stabilization ($T_H = \text{const}$).

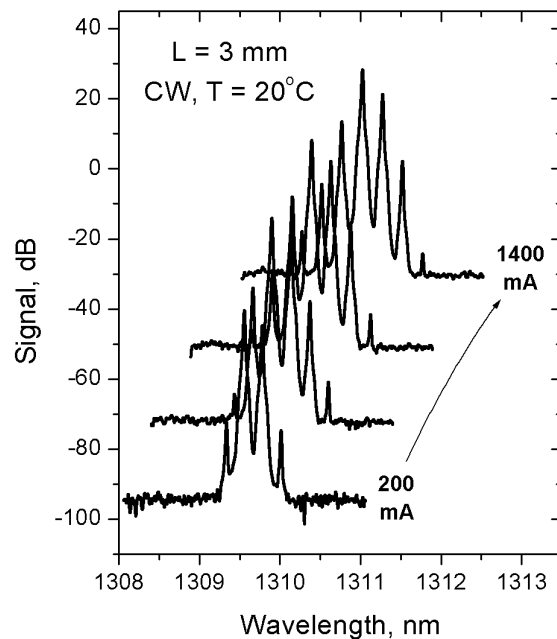


Fig.7. Spectral behavior of multi-frequency (group B) DFB laser with cavity length of 3 mm. Side mode suppression ratio increases from 45 dB at 200 mA to more than 60 dB at 1400 mA drive current.

Multi-frequency and single-frequency DFB lasers have almost identical P-I characteristics (Figs. 4, 6). Slope efficiencies of MF DFB lasers are slightly lower than that of SF emitters, and hence average maximum power of MF DFB lasers is 5-10% less than that of SM devices. Threshold current values and threshold temperature dependencies are similar for SF and MF lasers of the same cavity length.

An exponential fit of the temperature dependence of threshold current yields for low temperature range ($T < 50^\circ\text{C}$) a characteristic temperature (T_0) of 70-75 °C for 2 mm DFB, and 80-85 °C for 3 mm DFB and Fabry-Perot lasers. Above

45-50 °C, for 2 and 3 mm cavity DFB lasers, the thresholds become more temperature sensitive with the values of T_0 in the range of 20-40 °C. Threshold dependencies for Fabry-Perot lasers do not exhibit such a pronounced T_0 decrease in the high-temperature range. This difference in the behavior of DFB and Fabry-Perot lasers at high temperatures is most likely associated with the temperature-induced gain-peak – grating wavelength de-tuning. This effect leads to rapid threshold current rise for DFB emitters.

MF and SF emitters have the same output beam far-field patterns and consequently, similar single-mode fiber coupling efficiency. The typical far field distribution for a DFB laser is displayed in Fig. 9. FWHM for a fast axis divergence (about 26°) is independent of the drive current, while the slow axis FWHM divergence shows a modest increase with operating current, similar to the behavior of Fabry-Perot lasers. The value of lateral FWHM (8-10°) is lower for DFB lasers than for Fabry-Perot devices.

Fibers with a conventional lensed input end, as well as a simple aspherical lens pair (GelTech), have been used for DFB laser output power coupling into SMF-28 fiber. Despite the large aspect ratio of the laser beam, in both cases about 65% coupling efficiency has been achieved. Similarly to coupling efficiency of Fabry-Perot devices, the coupling efficiency of DFB lasers exhibits a modest increase with increasing drive current due to current-induced widening of the slow axis optical field distribution. More than 300 mW ex-fiber CW SF power has been achieved at 1.4 A.

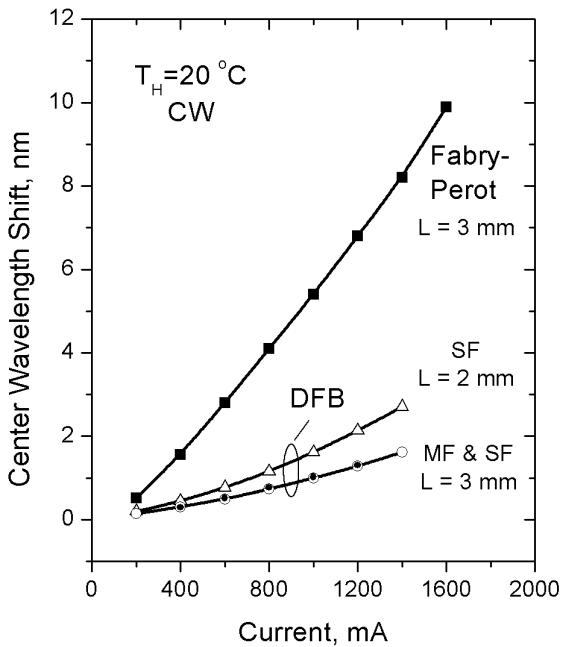


Fig.8. Current-induced wavelength shift for: Fabry-Perot laser (solid squares, $L = 3$ mm), SF DFB laser (open triangles, $L = 2$ mm), and SF DFB laser (open circles, $L = 3$ mm), and MF DFB laser (solid circles, $L = 3$ mm).

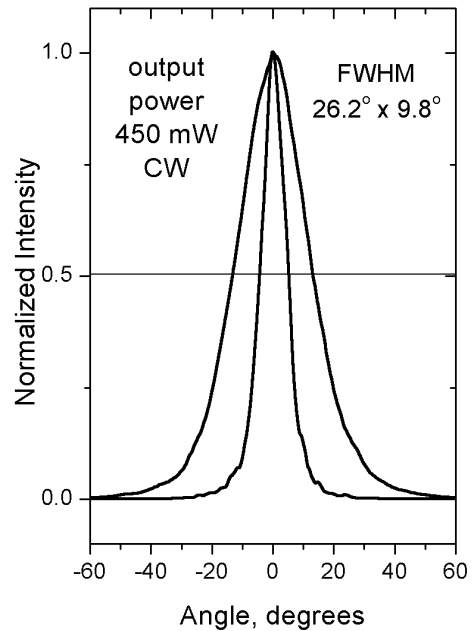


Fig.9. Slow and fast axis far-field radiation patterns of DFB laser with cavity length of 3 mm, measured at output power of 450 mW.

5. RELATIVE INTENSITY NOISE OF FABRY-PEROT AND DFB LASERS

High power 13xx nm DFB lasers can be used as both source lasers and as high-power pumps, when several lasers with different wavelengths should be combined using WDM technique. For lasers used in Raman amplifiers or transmitter systems, the spectral and noise characteristics are very important for system performance. The noise in the pumping system can lead to the increase of amplifier noise. Relative intensity noise (RIN) transfer characteristics for counter- and

co-pumping configurations of Raman amplifier have been recently considered [11]. It has been shown that in a certain frequency range, noise transfer coefficient can exceed 1. The region of frequencies with enhanced noise transfer is considerably broader for co-pumping (up to 5×10^7 Hz) amplifiers than that for counter-pumping Raman amplifiers (up to 5×10^3 Hz). As a result, the tolerable level of the average pump laser noise for co-pumping applications should be less than -110 dB/Hz, and less than -20 dB/Hz for counter-pumping applications.

Below we will consider the power-noise characteristics of high-power ridge waveguide 13xx nm Fabry-Perot and distributed feedback lasers [1]. The RF frequency block of the HP70001 analyzer used in our experiments puts a 10^5 Hz limit on the low frequency range of our measurements.

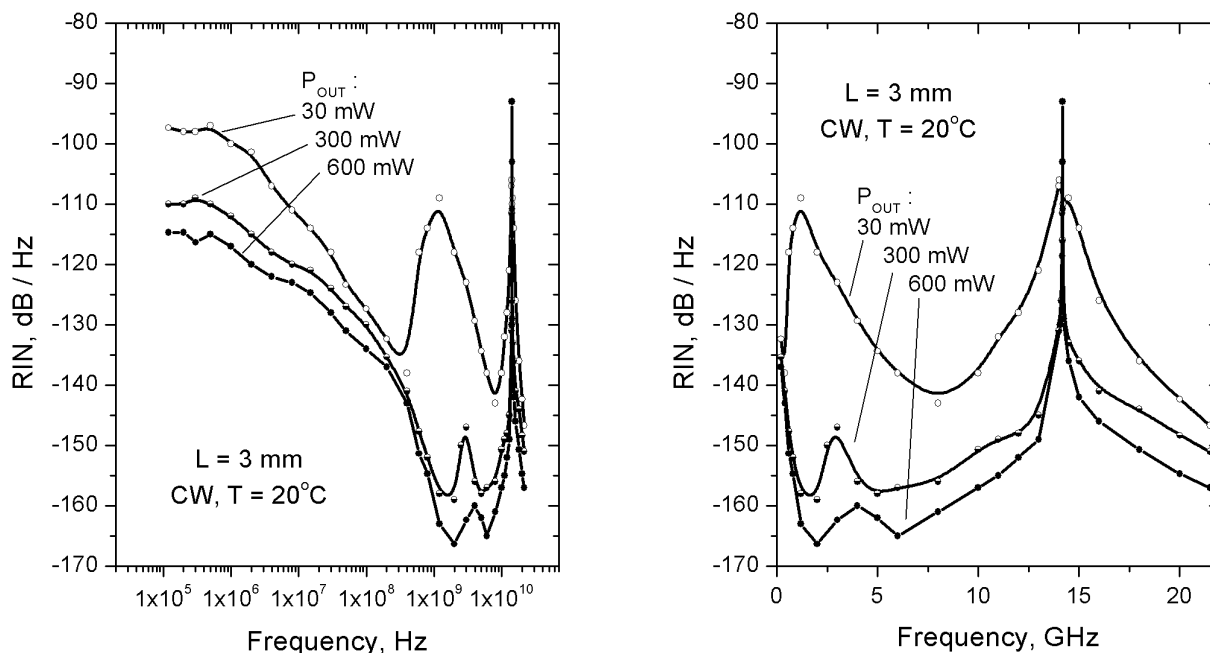


Fig. 10 (a, b). Relative intensity noise of a $\lambda=1310$ nm Fabry-Perot laser diode with 3 mm cavity length. Data were measured at three different current power levels of 30 mW, 300 mW, and 600 mW, corresponding to currents of 0.15A, 0.8A, and 2A, respectively. The RIN spectra are shown in logarithmic (a) and linear (b) frequency scales.

Figures 10(a) and 10(b) demonstrate relative the intensity noise for a $\lambda=1310$ nm Fabry-Perot laser diode with a 3 mm cavity length. The RIN was measured at three different power levels of 30 mW, 300 mW, and 600 mW, corresponding to currents of 0.15A, 0.8A, and 2A, respectively. The RIN spectra are shown in logarithmic (a) and linear (b) frequency scales to emphasise low frequency (a) and high frequency (b) RIN behaviour. The RIN values for Fabry-Perot at lower frequencies are mainly caused by mode-partition noise. Low frequency RIN gradually decreases with increasing output power, reaching -110 dB/Hz level at 300 mW output power (Fig. 10).

RIN peak associated with relaxation oscillations shifts from about 1 GHz at 30 mW output power to about 4 GHz at 600 mW with amplitude, decreasing from about -100 dB/Hz near the threshold down to -160 dB/Hz at maximum power.

The strongest peak of Fabry-Perot laser RIN spectra is the high frequency peak caused by the beating between N- and N+1 longitudinal modes. The position of this peak for 3 mm cavity lasers is located at 14 GHz, in accordance with simple relation: $f = c/2Ln$, where c is the speed of light in a vacuum, L is the device cavity length, and n is the effective group index of refraction of the RWG laser. In contrast to low frequency noise and relaxation oscillation noise, the noise associated with mode beating does not decrease with power increase.

RIN spectra for SF and MF DFB lasers, shown in Fig. 11 and 12, have features similar to those of Fabry-Perot devices. However, the RIN values are almost 30 dB less than that in the case of Fabry-Perot lasers. In the region of effective noise transfer (from 10^5 to 5×10^7 Hz), the RIN values for both types of DFB lasers are below -135 dB/Hz.

In Fig. 12, RIN spectra for high-power SF and MF DFB lasers with cavity lengths of 3 mm are compared. Low frequency RIN values for MF DFB are only a little higher than those for SF DFB devices. It allows us to assume that a contribution to the low frequency noise from DFB mode instability in MF devices is not large, and probably there is another source of low frequency noise, common for both types of DFB lasers.

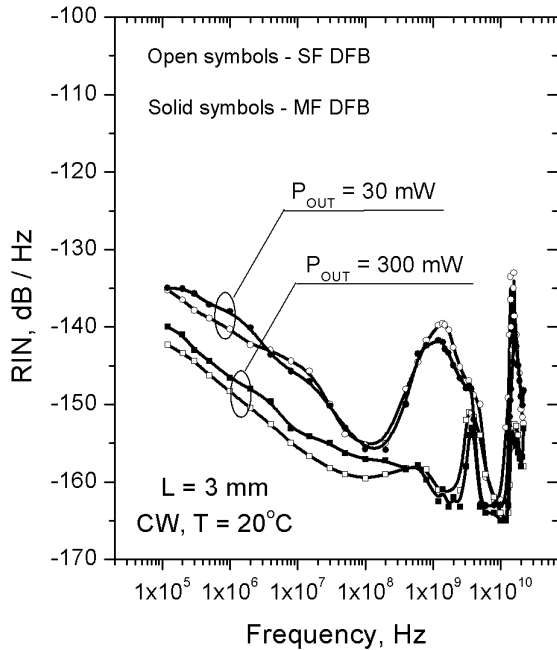


Fig.11. Relative intensity noise of a $\lambda=1310$ nm single-frequency (open symbols) and multi-frequency (solid symbols) DFB laser diodes with 3 mm cavity length. Data measured at two power levels of 30 mW and 300 mW, corresponding to currents of 0.14-0.16 A and 0.95-1.1A, respectively.

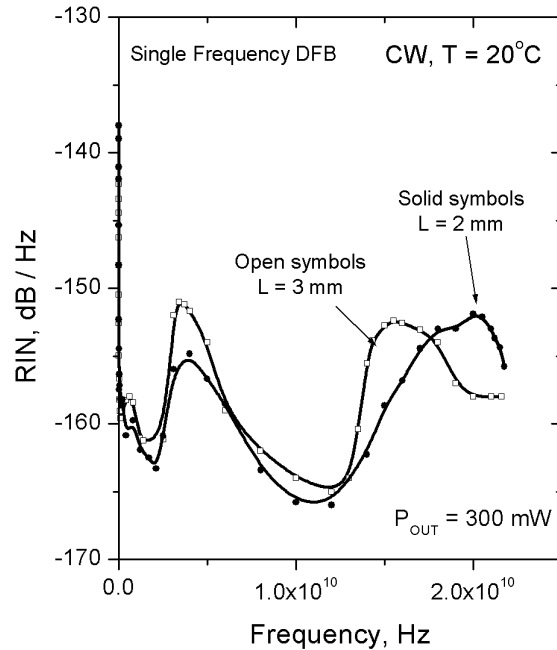


Fig.12. Relative intensity noise of a $\lambda=1310$ nm single-frequency DFB laser diodes with cavity length of 3 mm (open symbols) and 2 mm (solid symbols). Data measured at power level of 300 mW.

High frequency (>10 GHz) peak positions coincide for FP and DFB lasers of the same cavity length. In contrast to FP lasers, in the case of DFB lasers the intensity of this peak decreases with output power. RIN spectra for 2 mm and 3 mm SF DFB lasers, shown in Fig. 12, demonstrate the shift of high frequency peak to the higher frequency for DFBs with shorter cavities. These three features allow us to assume that the high frequency peaks in RIN spectra of DFB lasers are probably associated with beating between superluminescent modes of Fabry-Perot cavity.

6. CONCLUSION

Optimization of the ridge waveguide design allowed us to achieve more than 800 mW and 500 mW output power from 1310 nm single mode Fabry-Perot and DFB lasers, respectively. Despite the fact that the beam aspect ratio for ridge lasers is higher than that for buried heterostructure devices, our modeling and experiments demonstrated that the fiber coupling efficiency of about 75-80% could be routinely achieved using a lensed fiber or a simple lens pair. Fiber power of higher than 600 mW was displayed for Fabry-Perot lasers.

Single frequency and multi-frequency DFB lasers have been studied. Both types of DFB lasers exhibit very weak wavelength-temperature dependence typical for DFB devices, and RIN values of 30 dB lower than those for Fabry-Perot lasers.

Ridge Waveguide Fabry-Perot and DFB lasers can be used as pump sources for Raman amplifiers operating in the 1300 nm wavelength range, where use of EDFAs is not feasible. The single-frequency 1300 nm DFB lasers operating in the 500 mW power range are very attractive for new generation of the cable television transmission and local communication systems.

ACKNOWLEDGEMENT

The authors would like to thank S. Todorov, R. Radionova (Princeton Lightwave, Inc.), A. Tsekoun, G. Minina, L. Hammer, A. Triano, R. Matarese (Sarnoff Corporation) for helpful discussions, device fabrication and assistance in measurements..

REFERENCES

- [1]. R. Menna, A. Komissarov, M. Maiorov, V. Khalfin, A. Tsekoun, S. Todorov, J. Connolly and D. Garbuzov, "High Power single spatial and longitudinal mode 1310 nm InGaAsP/InP lasers with 450 mW CW output power for telecommunication applications", *27th European Conference on Optical Communication*, **Tu.B.1.6**, (IEEE/LEOS and EUREL, 2001)
- [2]. A. Mathur, M. Ziari, V. Agrawal, E. Kolev, "High power 1.3 μm DFB lasers", *Electron. Lett.* **34**, pp. 2334-2336 (1998). 315 mW 1.4A, 300 kHz, RWG.
- [3]. D. Garbuzov, R. Menna, A. Komissarov, M. Maiorov, V. Khalfin, A. Tsekoun, S. Todorov, J. Connolly "1400 – 1480 nm ridge wavelength pump lasers with 1 watt CW output power for EDFA and Raman amplification", *Optical Fiber Communication Conference postdeadline papers, OSA Technical Digest Series*, **PD18** (Optical Society of America, Washington, D.C., 2001)
- [4]. R. Menna, A. Komissarov, M. Maiorov, V. Khalfin, L. DiMarco, J. Connolly and D. Garbuzov, "High Power 1550 nm Distributed Feedback Lasers with 440 mW CW Output Power for Telecommunication Applications", *Conference on Lasers and Electro-Optics postdeadline papers*, **CPD12-1**, (IEEE/LEOS and OSA, 2001)
- [5]. S. Y. Hu, D. B. Young, J. C. Yi, D. Leonard, L. A. Coldren, "High efficiency and low threshold InGaAs/AlGaAs quantum-well lasers", *J. Appl. Phys.* **76**, 3932-3934 (1994)
- [6]. Y. Inaba, M. Kito, J. Ohya, M. Ishino, Y. Matsui, "High-output power operation of a 1.3 μm gain-coupled distributed feedback laser with narrow spectral linewidth", *Jpn. J. Appl. Phys.* **38(1-2B)**, pp. 1252-1255 (1999); Y. Inaba, M. Kito, J. Ohya, M. Ishino, Y. Matsui, "High output power and narrow spectral-linewidth operation of 1.3 μm gain-coupled DFB laser with InAsP buried absorptive grating", *IEEE Photon. Technol. Lett.* **10**, pp. 1220-1222 (1998)
- [7]. T. R. Chen, P. C. Chen, J. Ungar, N. Bar-Chaim, "High-power operation of multi-quantum well DFB lasers at 1.3 μm ", *Electron. Lett.* **31**, pp. 1344-1345 (1995).
- [8]. T. Higachi, T. Takeuchi, K. Morito, M. Matsuda, H. Soda, "High-temperature CW operation of InGaAsP-InP semi-insulating buried heterostructure lasers using reactive ion etching technique", *IEEE Photon. Technol. Lett.* **7**, pp. 828-829 (1995).
- [9]. T. Higashi, S. J. Sweeney, A. F. Phillips, A. R. Adams, E. P. O'Reilly, T. Uchida, T. Fujii, "Observation of reduced nonradiative current in 1.3- μm AlGaInAs-InP strained MQW laser", *IEEE Photon. Technol. Lett.* **11**, pp. 409-411 (1999); C.-C. Lin, M.-C. Wu, H.-P. Shiao, K.-S. Liu, "High-temperature, low threshold current, and uniform operation 1 \times 12 monolithic AlGaInAs/InP strain-compensated multiple quantum well laser array in 1.5 μm ", *IEEE Trans. Electron Devices* **46**, pp. 1614-1618 (1999).
- [10]. R. Nagarajan, J. E. Bowers, "High-speed lasers" pp. 177-290, in *Semiconductor Lasers*, edited By E. Kapon, Academic Press (1999).
- [11]. C.R.S. Fludger, V. Handerek, R.J.Mears, "Pump to signal RIN transfer in Raman fibre amplifiers", *Electron. Lett.* **37**, pp. 15-17 (2001)